The effect of pressure on lean premixed hydrogen-air flames

Martin Rieth[a,*], Andrea Gruber[b,c], Jacqueline H. Chen[a]

[a] *Combustion Research Facility, Sandia National Laboratories, Livermore (CA), USA*
[b] *Department of Energy and Process Engineering, Norwegian University of Science and Technology, Trondheim, Norway*
[c] *SINTEF Energy Research, Trondheim, Norway*

Abstract

The effect of pressure on the propagation of lean premixed hydrogen-air flames is investigated numerically with a hierarchy of canonical configurations including direct numerical simulations of turbulent flames in homogeneous isotropic turbulence. Thermo-diffusive instability and the ratio of turbulent to laminar burning velocity are found to be clearly amplified for increasing pressure. The observed amplification results from the combined effects of multi-dimensional geometrical features of the reaction front induced by stretch, chemical kinetics and flame speed / thickness sensitivity to preferential diffusion induced by the flame geometry. High-pressure flames exhibit stronger sensitivity to fast molecular diffusion of hydrogen into the reaction front of a reference freely-propagating flame that is nominally weaker at high pressure due to the greater relative importance of chain-termination. In this context, two-dimensional flames subjected to monochromatic velocity perturbations demonstrate locally enhanced flame speeds and reduced flame

*Corresponding Author
Email address: mrieth@sandia.gov (Martin Rieth)

thickness at high pressure in regions of curvature that are convex towards the reactants. Furthermore, it is found that a Peclet number definition, based on the ratio of diffusive to convective time scales, provides a satisfactory global representation of pressure effects upon thermo-diffusive instabilities of freely-propagating flames. Finally, employing a series of carefully designed direct numerical simulations, it is empirically demonstrated that very similar flame responses can be obtained at atmospheric and pressurized conditions by approximately matching a selection of four key parameters ($\mathrm{Le}_{\mathrm{eff}}$, Ze, Ma, Pe). This key finding demonstrates that the flame speed enhancement often observed at elevated pressure is *not* a pressure effect per se, but rather determined by the sensitivity of the flame to preferential diffusion (Pe) versus its own reactivity (Ze), with nominally 'weaker' flames showing stronger sensitivity.

Keywords: Hydrogen Combustion, High-pressure Combustion, Premixed Combustion, Thermo-diffusive Instability

1. Introduction

Present and future efforts to curb carbon dioxide emissions and reduce the dependence on fossil fuels must consider the continued need for large-scale, on-demand power generation and propulsion solutions [1]. In this context, it is becoming increasingly evident that carbon-free energy carriers, such as hydrogen and ammonia, can play a key role in many industrial applications, ranging from gas turbines to reciprocating engines. However, from the perspective of these applied combustion technologies, the desired fuel switch from hydrocarbon-based fuels to their carbon-free counterparts

represents a significant technical hurdle. In particular, the high reactivity of hydrogen-containing fuel blends poses design challenges in simultaneously achieving low emissions performance and static and dynamic flame stability (i.e., avoiding flashback [2–5] and thermo-acoustics instabilities [6, 7]). Moreover, an increasing body of empirical evidence suggests that these challenges, posed by hydrogen combustion, are significantly exacerbated at the high pressures typically required in industrial applications [8, 9].

From a fundamental combustion perspective, hydrogen represents a unique fuel because of its high specific energy and its fast molecular diffusion relative to the diffusion of heat, resulting in a Lewis number well below unity ($\mathrm{Le}_{\mathrm{H}_2} \sim 0.3$). The low Lewis number leads to lean hydrogen-air flames becoming thermo-diffusively unstable, resulting in cellular burning patterns that have been observed for non-unity Lewis number flames since the seminal studies by Zeldovich [10] and Markstein [11]. A number of early studies, mostly limited to atmospheric pressure conditions, have revealed the influence of unsteady flame stretch on the enhancement of the burning rate for sub-unity Lewis number mixtures. In these premixed flames, the burning rate is locally amplified by preferential diffusion of the highly diffusive deficient reactant in positively curved flame cusps (convex to the reactants side of the flame). Early theoretical studies [12] have suggested that these positively curved flame cusps play a crucial, rate-controlling role in turbulent premixed combustion of sub-unity Lewis number mixtures. Subsequent experimental investigations [13–15] and Direct Numerical Simulation (DNS) studies, incorporating a detailed description of chemical kinetics and molecular transport [16–20], have shown the pronounced effect of unsteady stretch

on the turbulent burning velocity of hydrogen-air flames.

All these studies concur on the fact that, in turbulent premixed hydrogen-air combustion, the interaction of preferential diffusion and unsteady stretch causes a strong correlation between the fuel consumption speed with both curvature and strain rate, consistent with diffusive–thermal theory. Diffusive–thermal effects result in substantial changes of flamelet speed, augmented by as much as five times compared to the undisturbed laminar flame for highly unstable mixtures, whereas the area-weighted mean fuel consumption speed is found to be more than twice as large as the corresponding laminar (nominal) value [17]. Additional investigations focusing on premixed hydrogen-air flames at fuel-lean conditions have shown that positively curved flame cusps can approach the conditions of critically stretched flames [21] and locally feature strongly reduced chemical time scales [22].

The vast majority of the above-cited works, aiming at detailed experimental measurements or accurate numerical predictions (DNS), have only considered atmospheric pressure conditions in order to avoid major complications in diagnostic infrastructure or excessive computational cost. Some experimental studies have investigated the effect of pressure on laminar and turbulent premixed flame propagation and have shown that the ratio of turbulent to laminar burning velocity, S_T/S_L, increases with pressure [23–26]. These experimentally-observed trends, however, are difficult to interpret as they result from the nonlinear interactions of chemical kinetics, hydrodynamic and thermo-diffusive instabilities and Reynolds number *cross-effects* (i.e., as Re increases with pressure, all else kept equal). Only a few studies have specifically focused on and systematically investigated the effect of

pressure in sub-unity Le flames. Venkateswaran et al. [27] considered the particular case of negative Markstein-length fuel blends for which burning intensity increases with stretch and reported an increase in burning rates at higher pressures. Berger et al. [28, 29] investigated intrinsic instabilities in two-dimensional freely-propagating flames and reported decreasing equivalence ratio, decreasing temperature and increasing pressure to amplify thermodiffusive instabilities. Recent direct numerical simulation (DNS) studies [30, 31] reported increased characteristic fractal dimensions for sub-unity Le, and thinner and more strongly burning reaction zones in flame elements convex towards the reactants for higher pressures. The DNS study by Lu and Yang [32] investigated the combined effect of increasing pressure and turbulence intensity on the turbulent burning velocity for lean hydrogen-air premixed combustion to obtain quasi-empirical model correlations of S_T/S_L versus u'/S_l. However, the authors of that study relied on definitions of thermal flame thickness and Karlovitz number not strictly compatible with pressure invariance and applied a linear velocity forcing method across the turbulent flame brush [32] with unclear consequences on the accuracy of the predicted turbulent burning rate. While these earlier DNS studies were limited to relatively low turbulence intensities, a recent DNS study has revealed that, even at very high turbulence intensities, the reaction front acceleration, already enhanced by fast molecular diffusion of molecular and atomic hydrogen acting at its positively and negatively curved segments, respectively, is further amplified with increasing pressure [33]. The results confirm the empirical trends and related significant challenges observed in industrial applications [8, 9]. The key findings reported in [33] are qualita-

tively illustrated in Fig. 1 summarizing the key differences due to the effect of pressure in hydrogen-enriched flames (other parameters remaining constant). Notably, the figure shows a significant difference between atmospheric and high-pressure conditions (everything else being equal) in the impact exerted by fast hydrogen diffusion into flame segments with convex (positive) curvature towards the reactants. While the atmospheric-pressure flame only exhibits weak super-adiabaticity and a significantly broadened preheat zone, the high-pressure flame exhibits localized equivalence ratio enrichment leading to strongly super-adiabatic conditions that accelerate and strengthen the flame front.

Based on these results, the objectives of the present study are threefold: 1) identify the rate-controlling physical mechanisms that affect the pressure scaling of the turbulent burning velocity for premixed lean hydrogen-air flames; 2) use these fundamental insights to develop a simple physics-based expression that captures the pressure scaling, incorporating a novel Peclet number definition applicable to different flow configurations; and 3) to demonstrate that the pressure scaling can be reproduced by scaling of the reactants temperature and equivalence ratio. The latter proposition implies that the fundamental characteristics and scaling behavior of high-pressure, non-unity Lewis number flames may be investigated in experiments and DNS calculations at atmospheric-pressure conditions with simpler and less costly methodologies.

The remainder of this paper is organized as follows. Section 2 describes the hierarchy of flow configurations and simulation codes. Section 3 summarizes earlier theoretical work and the present knowledge on the topic while

Section 4 presents and discusses results from the multi-dimensional direct numerical simulations. In Section 6 the main conclusions of the present study are summarized and suggestions for future work are made.

2. Numerical Methods and Flow Configurations

A comprehensive set of hierarchical premixed flame configurations have been simulated with both low-Mach and fully-compressible DNS solvers. The target configurations consist of laminar freely-propagating unperturbed flames (LFPUF), laminar strained flames (LSF), laminar freely-propagating flame (LFPF), mono-chromatically sheared laminar premixed flames (MSLF) and turbulent flames (TF) in two- and three-dimensional computational domains. The hierarchy of configurations permits the study of pressure effects on intrinsic, self-excited instabilities versus complex instabilities that emerge in the presence of external forcing (i.e., turbulent velocity fluctuations and stretch). These are listed in Tab. 1 which summarizes their main features.

Simulations in the former two configurations are performed with the low-Mach adaptive mesh refinement solver PeleLM (based on the method outlined in [34]). Simulations in the latter two configurations are performed using the compressible reacting flow solver S3D [35]. The choice of the different solvers is motivated by the characteristics of the different physical problems, i.e., low flow velocities and long integration times for the 2-D freely-propagating and monochromatically-forced flames, and higher flow velocities and shorter integration times for the 2-D and 3-D flames wrinkled by turbulence. The chemical kinetics software Cantera [36] is employed for all one-dimensional (1-D) supporting flame calculations, i.e., freely-propagating premixed laminar

Configuration		Dim.	Flow	Perturbation	Code
C1	LFPUF	1-D	Laminar	None	Cantera
C2	LSF	1-D	Laminar	Strain	Cantera
C3	LFPF	2-D	Laminar	Intrinsic	PeleLM
C4	MSLF	2-D	Laminar	Mono-chromatic shear	PeleLM
C5	TF	2-D/3-D	Turbulent	2-D/3-D turb. spectrum	S3D

Table 1: Overview of the premixed flame configurations investigated in the present study. LFPUF: laminar freely-propagating unperturbed flame, LSF: laminar strained flame, LFPF: laminar freely-propagating flame, MSLF: mono-chromatically sheared laminar flame, TF: turbulent flame.

flames & counterflow flames. All solvers employ a detailed representation of the chemical kinetics, based on the elementary reactions scheme by Li et al. [37], and a mixture-averaged transport model in order to provide an accurate representation of fast molecular diffusion of molecular and atomic hydrogen.

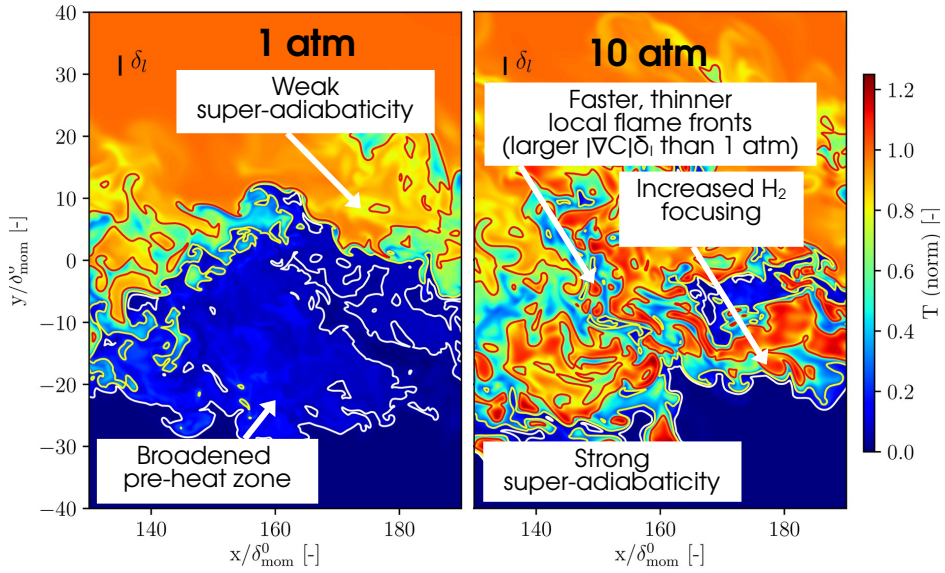

Figure 1: Instantaneous temperature contours from 3-D DNS of turbulent lean $NH_3/H_2/N_2$-air premixed flames nominally placed in same regime diagram location (broken reaction zones) at 1 and 10 bar [33]. The white, yellow and red isotherms correspond to 800 , 1000 and 1500 K. For reference the thermal flame thickness, δ_l, is shown.

3. Theory

Past experiments involving laminar spherically-expanding flames and related theoretical analysis indicate that the critical wave number (i.e., the wavenumber below which the flame becomes unstable) increases with pressure [38]. Also, very recent work [39] suggests that, even in the absence of thermo-diffusive effects, the pressure scaling of the critical wavenumber is steeper than that of the flame thickness, contrary to earlier assumptions [18, 40]. This can be attributed to an increase of the Zel'dovich number.

The development of predictive models for instabilities of laminar premixed flames has been attempted in the past but accurately predicting the thermo-

diffusive behavior of lean premixed hydrogen-air flames represents a notorious challenge and these models often fail to correctly capture the growth rates of the instability [41]. However, existing models such as the model by Matalon et al. [42], which is based the hydrodynamic theory of premixed flames, proved suitable for predicting critical wave numbers [41]. This model employs a dispersion relation formulated as:

$$\omega = \omega_{\mathrm{DL}} k \underbrace{-[B_1 + \mathrm{Ze}(\mathrm{Le}_{\mathrm{eff}} - 1)B_2 + \mathrm{Pr}B_3]}_{\omega_2} k^2 \tag{1}$$

where B_1, B_2 and B_3 depend on the temperature ratio, k is the (normalized) wave number and ω_{DL} the growth rate parameter of the hydrodynamic instability, see [42]. More recently, the quantity ω_2 from Eq. 1 has been used by Howarth & Aspden [43] to satisfactorily predict the evolution of thermo-diffusive instabilities in freely-propagating 2-D laminar flames.

Several earlier studies have identified different parameters that allow the characterization of the thermo-diffusive response of premixed flames, namely the Lewis number (Le, or effective Lewis number, $\mathrm{Le}_{\mathrm{eff}}$), relating mass and thermal diffusion, the Markstein number, Ma, characterizing the flame response to stretch, the Zel'dovich number (Ze), providing a measure of the global flame activation energy, and the Peclet number, Pe, comparing convective and diffusive mass transport and often used in the context of spherically expanding flames [18, 38, 42]. Figure 2 illustrates the pressure scaling of a few selected parameters extracted from unstrained, freely-propagating 1-D premixed laminar flames (Configuration C1 in Tab. 1) at an equivalence ratio $\phi = 0.3$ and reactants temperature, T_{u}=750 K (reference conditions). In the absence of pressure effects on the chemical kinetics and considering

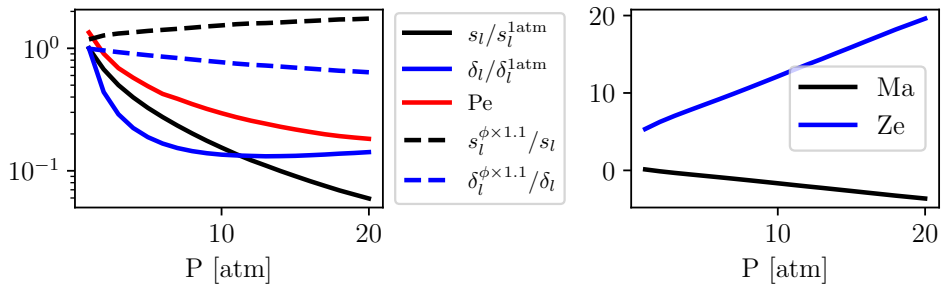

Figure 2: Pressure scaling of selected parameters in unstrained, freely-propagating 1-D premixed laminar hydrogen-air flames (C1) at reference conditions (T_u =750 K, ϕ =0.3). Left: laminar flame speed and thickness normalized by corresponding values at 1 bar ($s_l/s_l^{1\mathrm{atm}}$, $\delta_l/\delta_l^{1\mathrm{atm}}$), Peclet number (Pe) and flame speed and thickness sensitivity to equivalence ratio changes ($s_l^{\phi\times1.1}/s_l$ and $\delta_l^{\phi\times1.1}/\delta_l$, where the subscript $\phi\times1.1$ indicates a 10% increase of equivalence ratio). Right: Markstein (Ma) and Zel'dovich (Ze) numbers.

an overall reaction order of 2 (absence of termolecular reactions), laminar premixed flames scale as $\delta_l \propto 1/p$ and $s_l = \text{const.}$ [44]. However, three-body reactions, including the important chain-terminating elementary reaction, $H+O_2+M=HO_2+M$, are sensitive to increasing pressure levels. This leads to a decrease in the overall reaction order with increasing pressure (within the pressure range considered relevant in the present context), to a decrease in flame speed and to an increase in flame thickness relative to the $\delta_l \propto 1/p$ scaling [44] (i.e., a decrease in flame thickness to a lesser extent than $\delta_l \propto 1/p$). Notably, opposite trends compared to those discussed above are exhibited, for increasing pressure, by the *sensitivity* of flame speed and thickness to a marginal increase in the equivalence ratio. This is clearly illustrated in Fig. 2 by the dashed lines (compare with the solid ones) of the ratios $s_l^{\phi\times1.1}/s_l$ and $\delta_l^{\phi\times1.1}/\delta_l$ where the superscript $\phi\times1.1$ indicates a 10% increase of the equivalence ratio.

Across the pressure range considered in the present work (1-20 bar), the rate increase associated with chain-terminating reactions leads to a decrease in flame speed with increasing pressure, from 3.5 m/s at 1 bar to 0.23 m/s at 20 bar. Furthermore, the flame thickness monotonically decreases between 1 and 10 bar, from 500 µm at 1 bar to 68 µm at 10 bar, and then remains relatively unchanged for higher pressures up to 20 bar. Finally, the significant change in chemical kinetics is reflected in the change of Ze that increases almost linearly with pressure. This is a result of the cross-over temperature moving closer to the adiabatic flame temperature, i.e., the combustion process becomes nominally 'weaker'. Related to this behavior is the change in Pe, defined here as the ratio of convection to diffusion transport rates, based on 1-D calculations of unstrained premixed flames:

$$\begin{aligned} \mathrm{Pe} &= |\mathcal{C}_{\mathrm{H_2}}|_{\mathrm{1D,max}} / |\mathcal{D}_{\mathrm{H_2}}|_{\mathrm{1D,max}} \\ &= \frac{|\frac{\partial Y_{\mathrm{H_2}}}{\partial x} u|_{\mathrm{1D,max}}}{|\frac{1}{\rho}\frac{\partial}{\partial x}(\rho \frac{W_{\mathrm{H_2}}}{W_{\mathrm{m}}} D_{\mathrm{H_2}} \frac{\partial X_{\mathrm{H_2}}}{\partial x})|_{\mathrm{1D,max}}} \end{aligned} \tag{2}$$

where $|\mathcal{C}_{\mathrm{H_2}}|_{\mathrm{1D,max}}$ and $|\mathcal{D}_{\mathrm{H_2}}|_{\mathrm{1D,max}}$ are the maximum absolute values of convective and diffusive fluxes of H_2, respectively, $D_{\mathrm{H_2}}$ the species diffusion coefficient and $W_{\mathrm{H_2}}$ the molecular weight of H_2, respectively, W_{m} the mean mixture molecular weight and u the velocity. Note that the Peclet number definition given by Eq. 2 differs from the definition typically used in the literature. Most commonly, in this context, the Peclet number is defined on the basis of a critical radius in spherical flame experiments [18, 38, 42] while the present definition is extracted from simple calculations of one-dimensional laminar premixed flames. These can be conveniently performed using widely available open-source software such as Cantera [36]. Accordingly, the ra-

tionale behind the proposed expression for the Peclet number is to adopt a definition that is more general and not limited to specific configurations such as spherically expanding flames.

The inverse proportionality of Pe with respect to pressure implies that, as pressure increases, a gradual shift in the fundamental characteristic of the combustion process occurs with diffusion becoming more important relative to convection, ultimately resulting in a reduced flame speed. The reduction in Pe also implies that the combustion process becomes nominally 'weaker' with the flames moving closer to their lean flammability limit for increasing pressure.

Therefore, it is important to note that the aforementioned changes in Pe and Ze, with the related (nominal) weakening of the combustion process, are not only associated with an increase in pressure. Rather, similar effects on the flame characteristic parameters can be obtained by decreasing the reactants temperature T_u and equivalence ratio ϕ. The 'equivalence' between the effect of increased pressure and of decreased reactants temperature and equivalence ratio on the propagation characteristics of lean premixed hydrogen-air turbulent flames is demonstrated in the following section.

4. Results

4.1. Peclet Number and its Comparison to the ω_2 Parameter

In order to assess predictive capabilities of the definition of Pe proposed above, Eq. 2, the flame speed enhancement of freely-propagating 2-D laminar flames (Configuration C3 in Tab. 1) as a function of Pe are compared to the enhancement observed as a function of ω_2, shown in Fig. 3, for a set

of simulations originally presented by Howarth & Aspden [43]. These results are obtained from numerical simulations performed using the PeleLM code on computational domains extending $96\times\delta_l$ in x and y-directions, with three levels of grid refinement and a resolution of at least 16 grid cells per thermal flame thickness, as deemed sufficient for the evaluation of the fuel consumption speed, s_c, by Howarth & Aspden [43]. An initially planar flame is initialized normal to the x-direction such that it propagates in y-direction. The boundaries in y-direction are treated as inflow and outflow, with the inflow velocity being adjusted such that the flame remains inside the domain. Boundaries in x-direction are periodic. The unstable evolution of the 2-D freely-propagating flames is triggered by adding a small random perturbation of the initial flame position upon initialization. The flame speed s_c is calculated from data samples collected over a time period of 50 τ_l, starting at 50 τ_l after initialization.

It is observed that the parameters (inverse of) Pe and ω_2 provide similar scaling for s_c, suggesting that these can be used interchangeably with the former being a simpler model expression. This also relates the proposed expression for Pe to earlier modeling attempts [42]. For comparison, Fig. S1, provided in the Supplementary Material, illustrates the correlation of flame speed enhancement with the Zel'dovich and Markstein numbers, note the stronger relationship with the former compared to the latter. The parameter Pe provides a simple basis for the physical interpretation of a flame's thermo-diffusively unstable response: the preheat zone of a premixed flame is characterized by a balance of diffusion and convection, and the reaction zone by a balance of diffusion and reaction, which, depending on the condi-

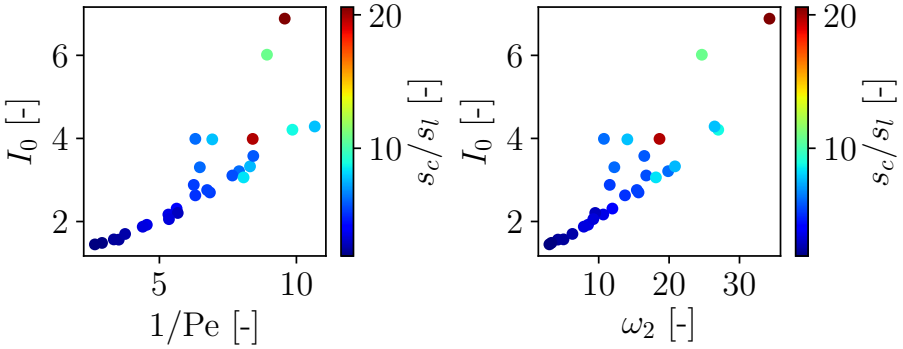

Figure 3: Stretch factor I_0 from 2-D laminar freely-propagating hydrogen-air flames (C3) versus 1/Pe (left) and ω_2 (right) for selected conditions (varying temperature, pressure and equivalence ratio) as in Howarth and Aspden [43] (see main text and Eq. 5 for a definition of I_0). Data points are colored by the fuel consumption speed.

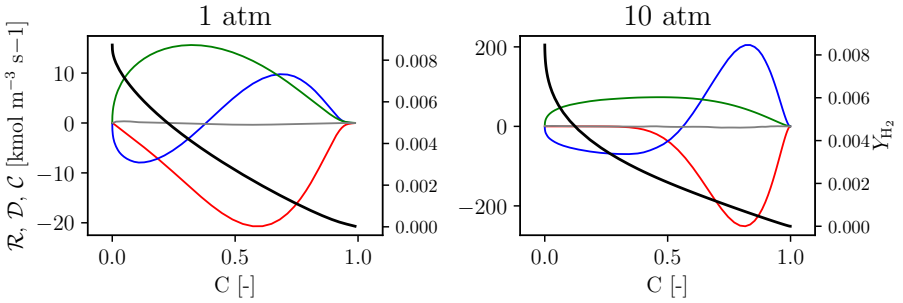

Figure 4: Reaction (red), diffusion (blue), convection (green) balance in progress variable space (here based on H_2O) for the fuel species (H_2) in 1-D lean premixed hydrogen-air laminar flames (C1) at 1 and 10 bar. The black lines show the hydrogen mass fraction Y_{H_2} profile.

tions, can also feature a contribution from convection. As the combustion process becomes weaker, i.e., through an increase in chain terminating reactions with pressure, the contribution of convective transport into the reaction

zone becomes smaller, while diffusion becomes more important (i.e., Pe as defined in Eq. 2 decreases). Figure 4 illustrates this situation by presenting reaction, diffusion and convection terms for the hydrogen mass fraction at 1 and 10 bar as a function of progress variable C, which is a parameterization of the reaction state that is equal to zero in the fresh reactants (C = 0) and unity in the burnt products (C = 1). Here C is based on the mass fraction of H_2O. A flame whose reaction zone becomes increasingly reliant on diffusion (i.e., for increasing pressure) will, as a consequence, react more strongly to geometrical perturbations of the flame surface that amplify diffusive effects, and hence it will feature a stronger thermo-diffusive instability. Furthermore, as shown in Fig. 4, the narrower fuel consumption layer (red line) at 10 bar is confined to higher progress variable values (≥ 0.5) and this may enable the upstream accumulation of fuel by molecular diffusion (local enrichment) if the necessary flame front curvature conditions are met. While this phenomenological picture is oversimplified, it illustrates the principal drivers of the flame thermo-diffusive response to increasing pressure. It should also be noted that the different response to pressure induces secondary effects. For example, the steepening of gradients in the flame structure, resulting from local enrichment, in turn, will further affect the convection-diffusion-reaction balance.

4.2. DNS Configurations and Parameters

The observation of similar flame responses obtained from different parametric variations (e.g., temperature, pressure) raises the question of whether the effects discussed above are uniquely a feature of pressure variations or

Case	P1	P10	P20	P1-10	P1-20	P10-1	P20-1
P	1	10	20	1	1	10	20
T_u	750	750	750	561	487	1058	1098
ϕ	0.3	0.3	0.3	0.23	0.22	0.31	0.37
u'/s_l	21.31	46.55	51.86	45.89	51.73	21.41	21.62
l_t/δ_l	2.25	4.91	5.47	4.84	5.45	2.26	2.28
η_K/δ_l	0.013	0.028	0.031	0.027	0.031	0.013	0.013
s_l	3.50	0.54	0.21	0.23	0.06	8.71	9.85
δ_l	5.0E-04	6.8E-05	7.1E-05	1.0E-03	2.4E-03	3.54E-05	1.67E-05
$\mathrm{Le_{eff}}$	0.43	0.39	0.38	0.37	0.36	0.44	0.46
Ze	5.3	12.1	19.6	12.1	20.1	4.8	5.1
Ma	0.13	-1.67	-3.63	-1.67	-3.65	0.12	0.12
Pe	1.35	0.30	0.18	0.29	0.15	1.64	1.58
ω_2	0.20	3.91	8.07	4.43	10.06	-0.02	0.00
I_0 (from C3)	1.00	1.52	2.05	1.59	2.21	0.99	0.87
δ/δ_l (from C3)	1.39	0.70	0.47	0.72	0.51	1.17	1.53

Table 2: Overview of 2-D/3-D DNS cases (C5). The parameters I_0 and δ/δ_l are obtained from laminar freely-propagating 2-D flames (i.e., without imposed turbulent velocity fluctuations, C3), ω_2 is calculated using the model by Matalon et al. [42]. All cases feature Ka = 300, $\mathrm{Re_t}$ = 1000 and Da = 0.1 (based on thermal flame thickness as in [45]). All cases are simulated in 2-D while only cases P1, P10 and P1-10 are simulated in 3-D.

whether the same thermo-diffusive flame response can be expected for a different combination of parameters at atmospheric pressure. This open question is explored in the discussion about 2-D wrinkled premixed laminar flames and 3-D turbulent premixed flames below. In order to investigate whether the flame response observed at high pressure conditions can also be obtained at atmospheric pressure, cases at 1 atm were designed by modifying unburned temperature, T_u, and equivalence ratio, ϕ, such that the set of parameters

$\mathrm{Le_{eff}}$, Ze, Ma and Pe, which are frequently used in theory and modeling [27, 38], matches closely the parameters obtained at elevated pressure and reference conditions (ϕ=0.3 and T_u=750 K). The effective Lewis number, $\mathrm{Le_{eff}}$, is computed based on Eq. 6 in [46]:

$$Le_{\mathrm{eff}} = 1 + \frac{(Le_{\mathrm{E}} - 1) + (Le_{\mathrm{D}} - 1)A}{1 + A} \tag{3}$$

where Le_{E} and Le_{D} are Lewis numbers for excess and deficient reactants, respectively. Parameter A depends on the Zel'dovich number, Ze, defined as $Ze = 4(T_b - T_u)/(T_b - T_0)$ (e.g., [39], with T_0 being the cross-over temperature). The Markstein number is defined as [47]:

$$\mathrm{Ma} = \gamma_1 + \gamma_2 Ze(Le_{\mathrm{eff}} - 1)/2, \tag{4}$$

using $\mathrm{Le_{eff}}$ from Eq. 3 and parameters γ_1 and γ_2, which depend on the thermal expansion parameter, T_b/T_u [47]. A range of T_{u} and ϕ was spanned in search of the conditions that match the desired conditions as closely as possible (in terms of the sum of absolute normalized errors of the four parameters). All parameters of the various cases studied in this work are given in Tab. 2. Cases at 750 K, $\phi = 0.3$ (baseline T_{u} and ϕ) and pressures of 1, 10 and 20 bar are denoted as P1, P10 and P20, respectively. Atmospheric pressure cases matching the conditions at 10 and 20 bar are denoted as P1-10 and P1-20, respectively. In addition, cases at 10 and 20 bar that match parameters at 1 bar are denoted as P10-1 and P20-1. Flames P1-10 and P1-20 have lower unburned temperature and equivalence ratio compared to flame P1, meaning that they move closer to the flammability limit (relative to P1) to "mimic" the effect of pressure at atmospheric conditions. Table 2 also includes the thermo-diffusive instability growth rate, ω_2, predicted by the

model of Matalon et al. [42] and employed by Howarth & Aspden [43] to construct their empirical model. The parameters I_0 and δ/δ_l represent the local burning rate enhancement (the stretch factor) and reduction in thermal flame thickness in laminar freely-propagating 2-D flames (Configuration C3 compared to 1-D laminar unperturbed flames of Configuration C1).

The stretch factor I_0, which accounts for the effects of flame stretch on the internal structure of the flame, is computed from the DNS data as originally suggested by Bray and Cant [48]:

$$I_0 = \frac{s_c}{s_l \sigma} = \frac{(\rho_u (Y_{\mathrm{H_2,b}} - Y_{\mathrm{H_2,u}}))^{-1} \int_0^L \langle \dot{\omega}_{\mathrm{H_2}} \rangle dx}{s_l \int_0^L \langle |\nabla C| \rangle dx}, \tag{5}$$

where s_c is the consumption speed and σ the flame surface area ratio. Angled brackets denote averaging orthogonally to the propagation direction with the integration performed over the domain length in the propagation direction (L). As such, the quantity I_0 represents the ratio between the (actual) global fuel consumption rate, integrated over the computational volume, and the (hypothetical) fuel consumption rate of an idealized laminar flame that has undergone the same flame area increase as the turbulent one. The stretch factor has been found to be near unity for thermo-diffusively neutral mixtures, i.e., $Le = 1$, but increases for mixtures characterized by sub-unity Lewis numbers through preferential diffusion [49, 50]. Hence, values of I_0 that significantly exceed unity represent the quantification of the extent to which increments of the turbulent burning rate, in thermo-diffusively unstable flames, are controlled by changes to the local flame structure, through localized enrichment and enhanced burning, relative to the "conventional" acceleration mechanism, governed by flame surface area generation.

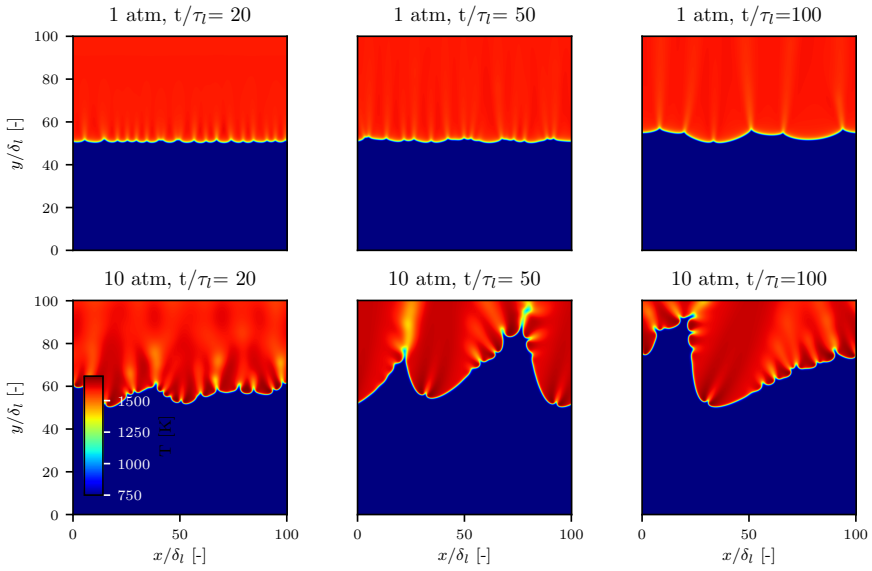

Figure 5: Evolution of the temperature field in two-dimensional freely-propagating flames (C3) at 1 and 10 atm (corresponding to conditions of P1 and P10 from Tab. 2).

An additional set of two-dimensional, freely-propagating laminar flames (Configuration C3 in Tab. 1) are calculated at the target thermo-chemical conditions listed in 2. This is to precisely assess, through the quantities I_0 and δ/δ_l, the characteristics of *intrinsic* (i.e., no external forcing by turbulence) thermo-diffusive instabilities that these flames exhibit at the thermo-chemical conditions listed in Tab. 2. The sequences in Fig. 5 qualitatively illustrate the temporal evolution of the instantaneous temperature field in two of the cases simulated, at conditions of P1 and P10. A numerical procedure similar to that described in Sec. 4.1 for Configuration C3 is employed, but here featuring domain sizes of $100\times\delta_l$ (δ_l based on premixed unstrained 1-D flames) in both x and y-directions, two levels of grid refinement across the flame thickness and a resolution of 32 grid cells per laminar flame thick-

ness. The quantities I_0 and δ/δ_l, relating fuel consumption rates and flame thicknesses for the freely-propagating 2-D flames to those of unperturbed 1-D premixed flames, are obtained by averaging data samples over a time period of 50 τ_l, starting at 50 τ_l after initialization, and are listed in Tab. 2. Here, flame thicknesses are extracted by averaging over randomly selected flamelets. As expected (from ω_2), the quantity I_0 in case P1 remains close to unity (slightly exceeding it) while in cases P10 and P20 I_0 is amplified, reaching 1.51 and 2.05, respectively. Clearly, flames from cases P10 and P20 are more thermo-diffusively unstable compared to the flame from case P1, with the instability becoming stronger with pressure, as predicted by the model by Matalon et al. [42]. It can also be observed that flames with parameters matching those at different pressures (P1-10, P1-20, P10-1 and P20-1) behave similarly to their counterparts. It should be noted that no particular attention is given in this discussion to the hydrodynamic instability since, based on the work by Chaudhuri et al. [51], the hydrodynamic instability is not expected to play a significant role for the high turbulence intensity conditions targeted. A discussion about 2-D and 3-D DNS of the turbulent flames listed in Tab. 2 follows in Sec. 4.5 after an analysis of simpler 1-D and 2-D strained flames is presented in Sec. 4.3 and Sec. 4.4.

4.3. 1-D lean premixed hydrogen-air laminar flames subject to linear strain

In order to assess differences in flame response to strain for increasing pressure, calculations of one-dimensional, steady-state laminar counterflow flames in a reactants-to-products arrangement (configuration C2 in Tab. 1) are performed, as illustrated in Fig. 6, and analyzed at strain rates that

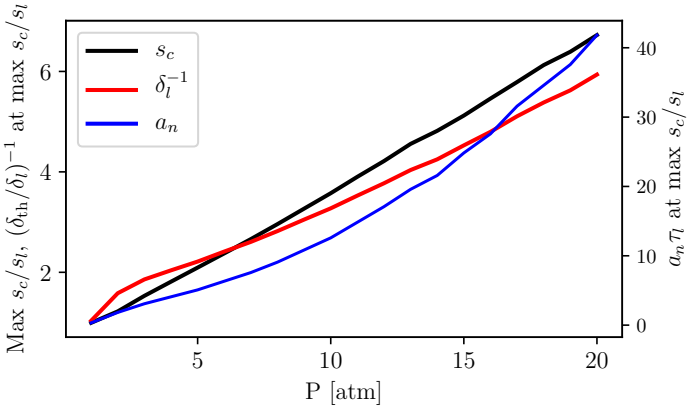

Figure 6: Peak normalized fuel consumption speed, s_c/s_l, reciprocal of normalized thermal flame thickness, $(\delta_{\mathrm{th}}/\delta_l)^{-1}$, and normalized global normal strain, $a_n\tau_l$, in steady-state laminar counterflow flames for varying pressures (C2). All flames are simulated at reference conditions $\phi = 0.3$ and $\mathrm{T_u}$=750 K.

correspond to the largest fuel consumption rate at each pressure level considered. For increasing pressure, peak fuel consumption rates increase and the flame thickness decreases, implying that the flame response to strain is amplified at elevated pressure, a behavior that is related to the Markstein number. Between 1 and 20 bar, the Markstein number decreases from 0.13 to -3.65, accounting for the behavior of s_c/s_l with strain. Differences in response to strain have obvious implications for turbulent flames at these conditions. High-pressure flames will respond more strongly to turbulence-induced strain/stretch by faster propagation of a thinner reaction front. In turn, this suggests that flames at elevated pressure become more strain resilient and less prone to extinction, confirming earlier findings from DNS of turbulent high-Ka premixed flames [33].

4.4. 2-D lean premixed hydrogen-air laminar flames subject to monochromatic shear

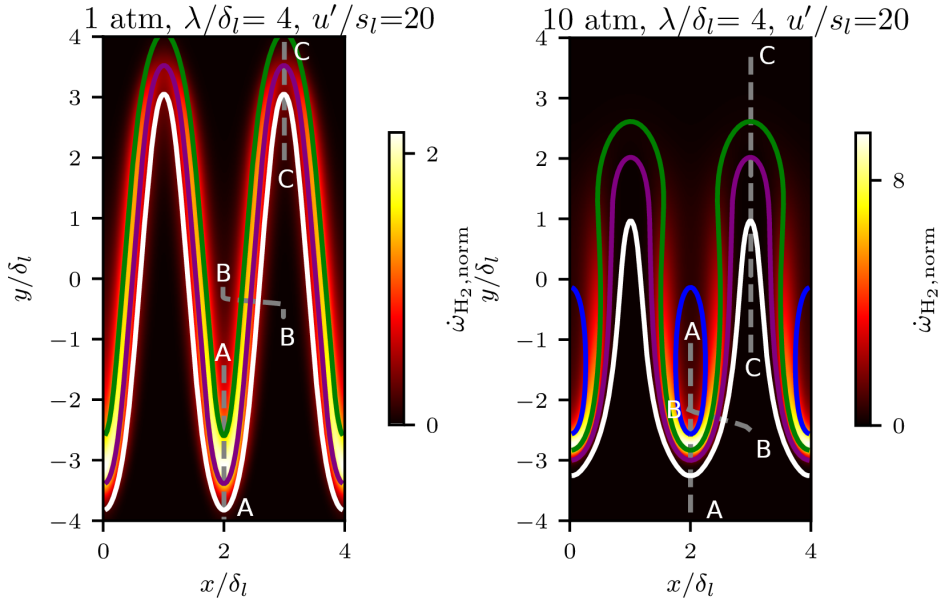

Figure 7: Exemplary normalized fuel consumption rate isocontours for the 2-D monochromatically-sheared laminar flames (C4) at 1 and 10 bar with λ/δ_l=4 and u'/s_l=20. The dashed grey lines represent selected flamelets extracted for analysis (positively curved (A-A), positively stretched with negligible curvature (B-B) and negatively curved flame elements (C-C)). White, purple, green and blue iso-lines correspond to normalized temperatures of 0.2, 0.5, 0.8 and 1.1 (superadiabatic).

Initially planar 2-D premixed hydrogen-air laminar flames are subjected to *monochromatic shear* (Configuration C4 in Tab. 1), i.e., sinusoidal velocity perturbation characterized by a constant wavelength and frequency, in order to investigate the effect of precisely controlled shear and resulting curvature of the reaction front. This configuration is similar to the configuration proposed by Feng et al. [52] to mimic flame propagation in boundary-layer turbulence.

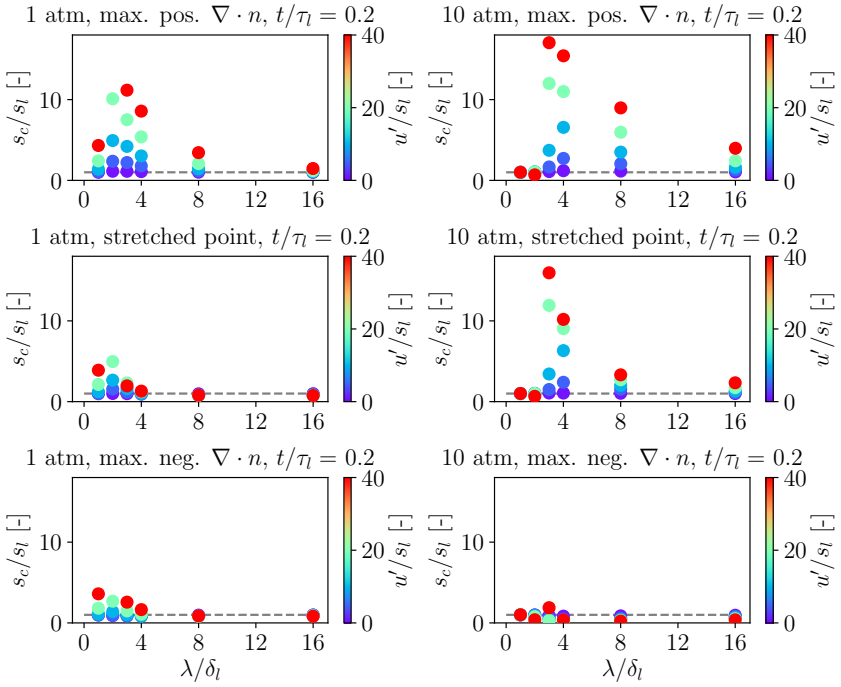

Figure 8: Normalized fuel consumption rate s_c/s_l versus normalized perturbation wavelength and velocity, λ/δ_l and u'/s_l, for flamelets extracted from 2-D monochromatically-sheared laminar flames (C4). The flamelet data shown here corresponds to the flamelets marked in Fig. 7 and it is sampled at points of maximum positive (A-A) and negative (C-C) curvature ($\nabla \cdot n$) and of maximum stretch (B-B), at 1 and 10 bar

Figure 7 shows exemplary cases of the normalized fuel consumption rate at 1 and 10 bar with a perturbation length scale, λ/δ_l, of 4 and a velocity perturbation, u'/s_l, equal to 20. This corresponds to u'/s_l approximately equal to that of case P1 and λ/δ_l close to the value that results in the strongest response to perturbations. Various length and velocity scales have been simulated ($\lambda/\delta_l \in [1, 2, 3, 4, 8, 16]$, $u'/s_l \in [1, 5, 10, 20, 40]$). In order to analyze the local effects of pressure in more detail, 1-D flamelets have been extracted from the 2-D simulations at different locations corresponding to the

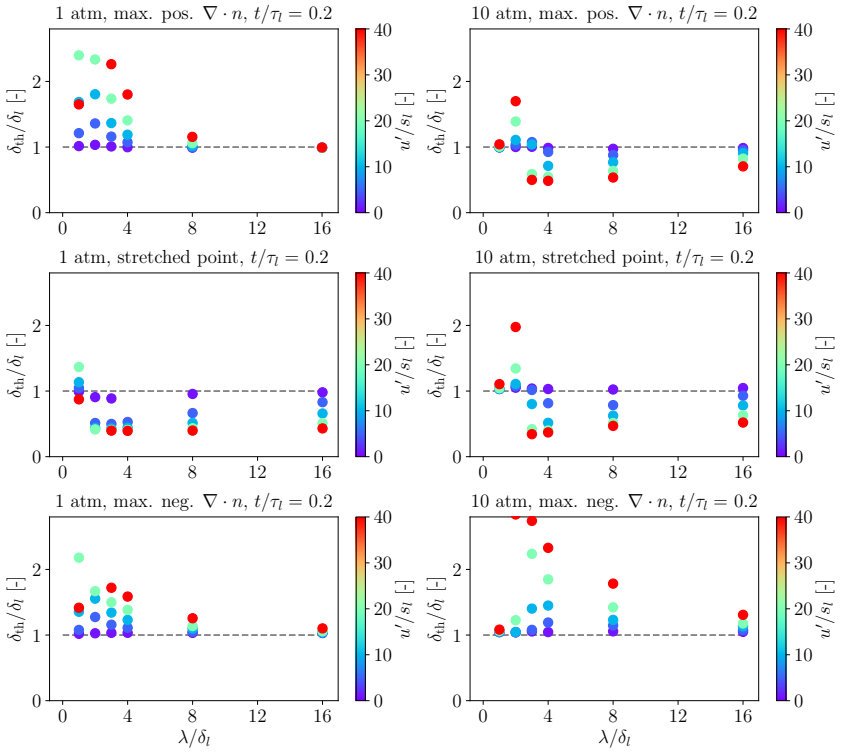

Figure 9: Normalized thermal flame thickness δ_{th} versus normalized perturbation wavelength and velocity, λ/δ_l and u'/s_l, for flamelets extracted from 2-D monochromatically-sheared laminar flames (C4). The flamelet data shown here corresponds to the flamelets marked in Fig. 7 and it is sampled at points of maximum positive (A-A) and negative (C-C) curvature ($\nabla \cdot n$) and of maximum stretch (B-B), at 1 and 10 bar

most positively curved point with a convex bulge with respect to the reactants (A-A), the most negatively curved point with a convex bulge with respect to the burnt products (C-C), and intermediate locations in between (B-B). The normalized fuel consumption rate s_c/s_l for the selected 1-D flamelets is shown in Fig. 8 whereas the corresponding thermal flame thicknesses are shown in Fig. 9. The chosen configuration allows for analysis of the steady flame response to perturbations characterized by a single well-defined length

and velocity scale, providing insight into expected flame behavior in the case of turbulent reactive flows that contain a broadband spectrum of scales.

As shown in the figures, s_c/s_l at the positively curved cusp (A-A) is strongly enhanced for both 1 and 10 bar, with a significantly larger amplification at 10 bar. Additionally, the high-pressure case shows signs of strong super-adiabaticity (Fig. 7). It is interesting to note that the 10 bar case exhibits a large s_c/s_l amplification at larger length scales ($\lambda/\delta_l \geq 8$) than the 1 bar case. On the contrary, length scales $\lambda/\delta_l \leq 2$ are not amplified at 10 bar while they are weakly amplified at 1 bar. More striking differences can be observed for the highly stretched intermediate flamelets (B-B) located between the positively- and negatively cuved cusps. At 10 bar, a very large s_c/s_l amplification is observed for $\lambda/\delta_l \sim 4$ while at atmospheric pressure only a marginal s_c/s_l enhancement is present. However, it should be noted that differences for the intermediate flamelet could be attributable to the super-adiabatic back support at 10 bar or to differences in stretch encountered at the selected flamelet positions, also with respect to the critical stretch rate for the 1 and 10 bar pressure conditions. Also, flame elements extracted at positively curved cusps (A-A) and intermediate locations (B-B) exhibit strongly enhanced burning rate at 10 bar while flamelets at negatively curved cusps (C-C) are characterized by an overall reduction of s_c/s_l.

Comparison of the thermal flame thickness response to shear also reveals interesting and important differences between 1 and 10 bar. While flamelets extracted in correspondence of positively curved cusps (A-A) become thicker in response to shear at atmospheric pressure, they become significantly thinner at 10 bar due to localized enrichment of the reaction layer (see preceding

sections). In a turbulent flow field, this phenomenon would cause positively curved flame elements not only to propagate faster but also to become thinner, ultimately resulting in a further enhancement of diffusive transport and leading to higher (and faster) local enrichment of the reaction layer until saturation is reached. The highly stretched intermediate-locations flamelets (B-B) become thinner both at 1 and 10 bar, whereas the flamelets from negatively curved cusps (C-C) become thicker.

In summary, the observed flame response to monochromatic shear with respect to stronger super-adiabaticity, smaller thickness of the reaction layer and augmented fuel consumption rate is qualitatively consistent with earlier findings from 3-D DNS of high-Ka turbulent $NH_3/H_2/N_2$-air flames at 1 and 10 bar [33]. However, it should be noted that in a turbulent flame the response to unsteady stretch becomes important, with stretch effects having been shown to attenuate when unsteady frequency and inverse of characteristic flame time become comparable [53]. An investigation of unsteady strain effects will be part of future work.

4.5. 2-D and 3-D flames subject to homogeneous isotropic turbulence

Building upon the results presented in the previous sections, an assessment of the turbulent reaction front response to pressure variations is attempted using more realistic, yet computationally tractable, DNS cases in two and three spatial dimensions (Configuration C5 in Tab. 1). Initially-planar, laminar premixed hydrogen-air flames, distributed across seven different two-dimensional DNS cases (see Tab. 2 for an overview), are subjected to pseudo-turbulent synthetic flow fields. Moreover, for three selected exem-

plary cases (P1, P10 and P1-10), the flames are subjected to more realistic three-dimensional homogeneous isotropic turbulence. The main parameters that characterize the turbulence-chemistry interaction for all cases considered in the present study are listed in Tab. 2. All turbulent reactive flows are simulated with the S3D code and feature a Karlovitz number Ka of 300, a turbulent Reynolds number $\mathrm{Re_t}$ of 1000 and a Damköhler number Da of 0.1, where these parameters are based on the thermal flame thickness instead of the Zel'dovich or related flame thickness (see [45] and [38] in the context of thermo-diffusive instabilities). Also, all two-dimensional cases are set up in a square computational domain with $L_x = L_y = 20 \times L_{\mathrm{int}}$, where L_{int} is the integral length scale. The spatial resolution is set to $\Delta x = \Delta y = \min(\delta_l/20, 2\eta_K)$, where η_K is the Kolmogorov length scale. The synthetic turbulent flow fields are initialized with a two-dimensional Passot-Pouquet spectrum. In the y-direction, non-reflecting outflow boundary conditions are imposed while cyclic conditions are imposed in the (periodic) x-direction. Initially flat laminar premixed flames are initialized with the flame normal aligned with the y-direction. The 3-D cases are set up in a similar fashion, with the additional extension of the computational domain in the (periodic) z-direction. In order to optimize the computational cost of the 3-D simulations, while still providing a sufficient amount of data samples for the accumulation of reliable statistics, the domain size in x- and z-directions are set to a quarter of the size compared to the y-direction, i.e., the non-periodic direction of flame propagation, which conserves its extension from the 2-D simulation equal to $L_y = 20 \times L_{\mathrm{int}}$. The spatial resolution requirements of the DNS dictate a total number of grid points in the y-direction between 1800 and

2200, leading to a typical total number of 4 M and 500 M grid points for the 2-D and 3-D cases, respectively.

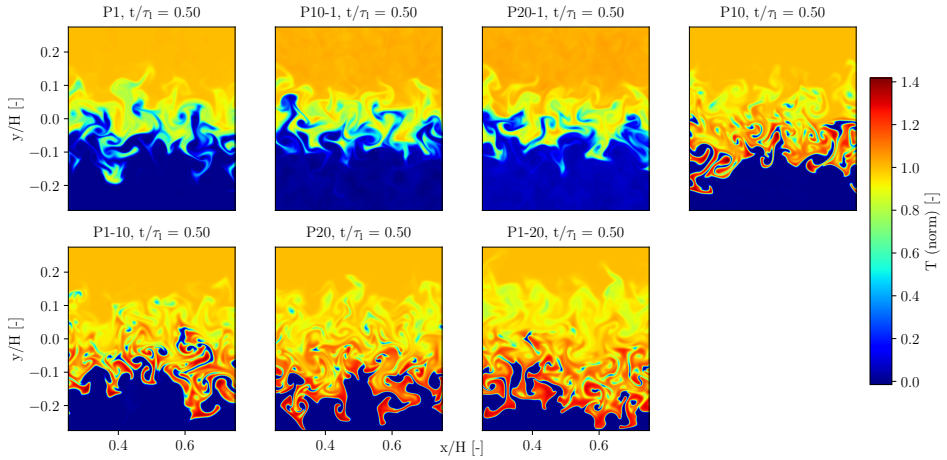

Figure 10: Normalized temperature fields at $t/\tau_l = 0.5$ for the 2-D cases P1, P10, P1-10, P20, P1-20, P10-1 and P20-1 (C5). Please refer to Tab. 2 for a summary of all cases presented.

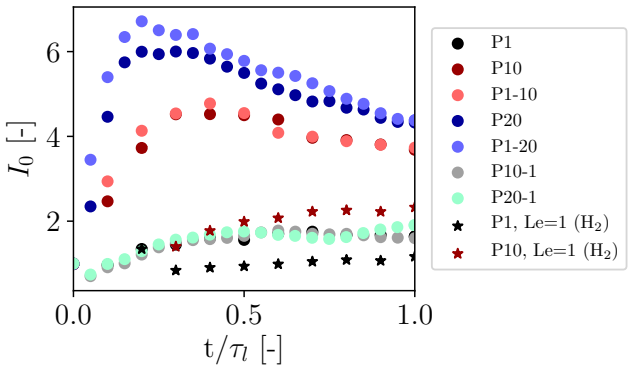

Figure 11: I_0 vs. normalized time for the 2-D cases P1, P10, P20, P1-10 and P1-20 (C5).

By design, in the absence of any thermo-diffusive instability, all simulated flames would behave similarly since they all nominally fall within the same combustion regime (based on a conventional definition for the regime

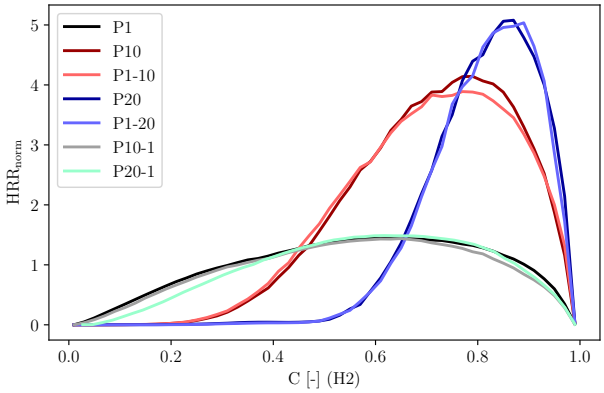

Figure 12: Normalized heat release rate conditioned on progress variable (here based on H_2) for the 2-D cases P1, P10, P20, P1-10 and P1-20 at t/τ_l=0.5 (C5).

diagram, e.g., [54]). Figure 10 illustrates the normalized temperature field evolved, for all cases, until a normalized time of $t/\tau_l = 0.5$. Please note that, except for a very short initial relaxation period, all of the following statements remain true when considering times preceding or following $t/\tau_l = 0.5$ (even though velocity fluctuations and turbulence intensities decay at late times).

In case P1, the 2-D pseudo-turbulent flow field wrinkles the reaction front with widespread disruption of the flame structure and significant broadening of the preheat layer by upstream turbulent transport of preheated material. For a phenomenological description of this situation see Fig. 2.11 in [54] and related discussion therein. The absence of strong super-adiabaticity in positively curved flame elements is also evident. Conversely, at the higher pressure levels, for 10 bar (case P10) and 20 bar (case P20), the wrinkled reaction fronts exhibit strongly super-adiabatic, intensely burning flame elements with positive curvature and the occurrence of fast-propagating, elongated

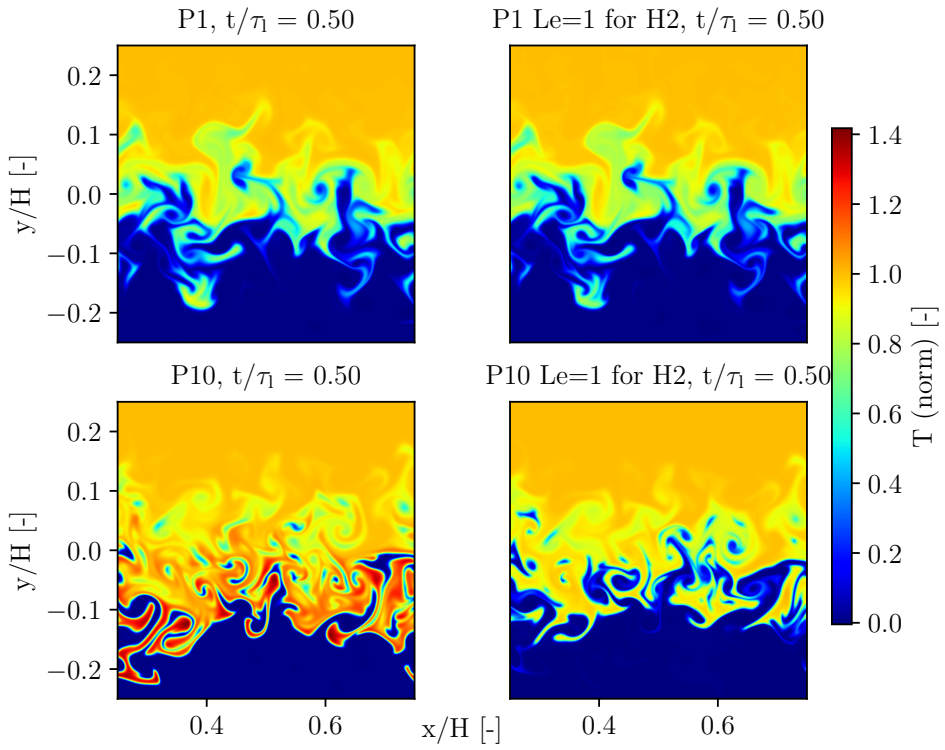

Figure 13: Instantaneous normalized temperature fields at $t/\tau_l = 0.5$ for the 2-D cases P1 and P10 and corresponding simulations that impose $\mathrm{Le}_{H_2} = 1$ (C5).

finger-like structures is observed.

As hypothesized, the evolution of the turbulence-chemistry interaction in case P1-10 and case P1-20 (atmospheric pressure cases designed to mimic high-pressure ones) are qualitatively very similar to case P10 and case P20, respectively, in terms of strong super-adiabaticity and fast displacement velocity of the positively curved flame elements. Likewise, case P10-1 and case P20-1 (high-pressure cases designed to mimic the flame evolution at atmospheric pressure), characterized by higher reactants temperature and equivalence ratio, feature broadening of the preheat layer and weak super-

adiabaticity.

Figure 11 presents the time evolution of I_0 for all seven cases listed in Tab. 2, as well as additional simulations configured to artificially enforce $\mathrm{Le} = 1$ for the H_2 species, which will be discussed below. Consistent with the temperature isocontours in Fig. 10, the increase in fuel consumption speed and flame surface density with time is amplified such that I_0 is significantly larger at higher pressure. Furthermore, all cases configured with matching parameters (P1-10, P1-20, P10-1 and P20-1) behave similar to the corresponding baseline cases at elevated or atmospheric pressures, respectively. Clearly, I_0 increases to a larger degree than in the laminar freely-propagating two-dimensional flames (C3) discussed above (Sec. 4.2, Tab. 2).

An assessment of the local flame structure alteration by turbulence-induced wrinkling is provided in Fig. 12 that shows conditional means of heat release rate versus progress variable. Similar to the behavior observed in Fig. 11, heat release rates are more strongly amplified in the higher pressure cases. Again, all cases configured with matching parameters (P1-10, P1-20, P10-1 and P20-1) show very similar conditional heat release rate statistics as their corresponding baseline counterparts, indicating that the turbulence-chemistry interaction is very similar in cases with matching governing parameters.

Figure 11 illustrates the temporal evolution of I_0 for calculations nominally identical to cases P1 and P10 except for the Lewis number of the H_2 species that is set to unity at a normalized time $t/\tau_l = 0.2$ (star-marked I_0 values). This numerical experiment allows an assessment of the turbulence-chemistry interaction response to the artificial removal of fast molecular diffusion of the H_2 species, in a situation where super-adiabaticity and local

enrichment of positively curved flame elements have already occurred. Figure 13 illustrates the instantaneous normalized temperature contours corresponding to a normalized time $t/\tau_l = 0.5$ (i.e., 0.3 t/τ_l after implementation of the $\mathrm{Le}_{\mathrm{H_2}} = 1$ condition). As evidenced by the figure, while the absence of fast molecular diffusion of the hydrogen fuel species at atmospheric pressure conditions produces few visible (very weak) differences, a significantly slower and colder flame develops at higher pressure (10 bar) for $\mathrm{Le}_{\mathrm{H_2}} = 1$. This observation bolsters the hypothesis that local enrichment caused by fast molecular diffusion of hydrogen has a stronger effect on flame propagation at higher pressure, due to the higher sensitivity to local enrichment of the positively curved flame elements.

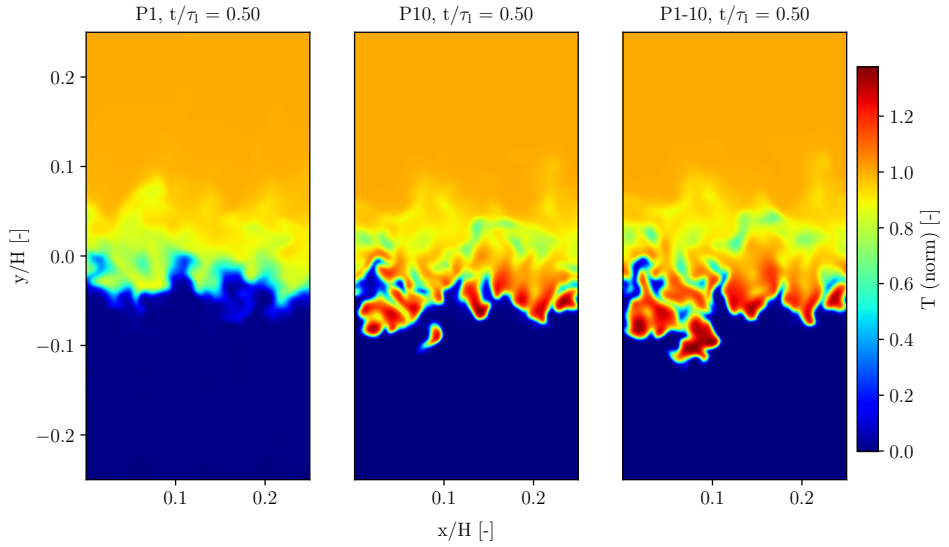

Figure 14: Normalized temperature fields at $t/\tau_l = 0.5$ for the 3-D cases P1, P10, P1-10 (C5).

In order to confirm the above observations from the 2-D DNS in more realistic turbulence-chemistry interaction configurations, three out of the seven

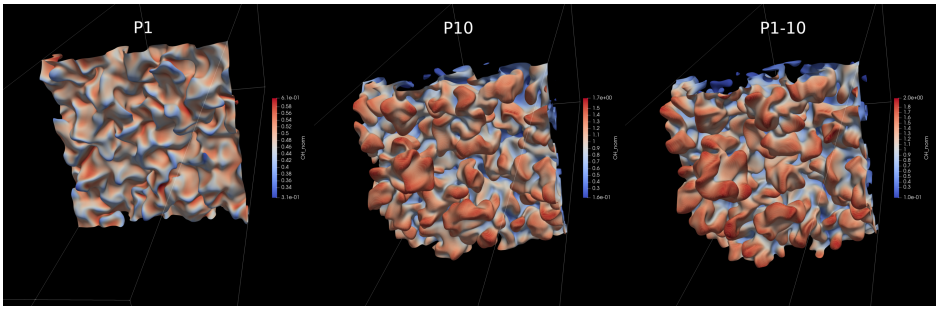

Figure 15: Temperature iso-contour (at maximum heat release rate in reference laminar flame) colored by normalized OH mass fraction at $t/\tau_l = 0.5$ for the 3-D cases P1, P10, P1-10 (C5).

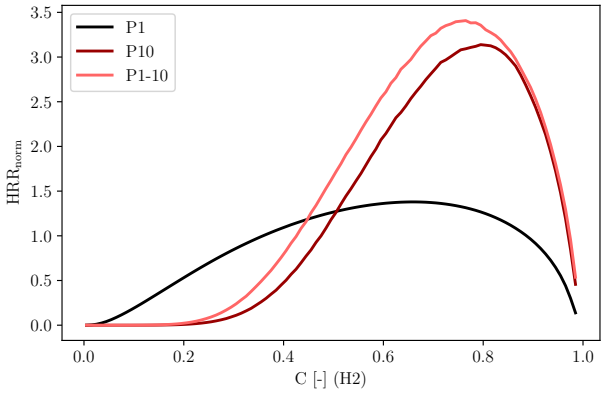

Figure 16: Heat release rate conditioned on progress variable (here based on H_2) for cases for the 3-D cases P1, P10, P1-10 at $t/\tau_l = 0.5$ (C5).

DNS cases are run in a 3-D configuration (P1, P10 and P1-10). Figure 14 qualitatively illustrates the main features of three-dimensional flames with instantaneous snapshots of the normalized temperature field at $t/\tau_l = 0.5$. Likewise, Fig. 15 presents corresponding three-dimensional volume renderings in which the iso-surface of temperature is shown. The temperature iso-surfaces correspond to the maximum heat release rate of the unperturbed

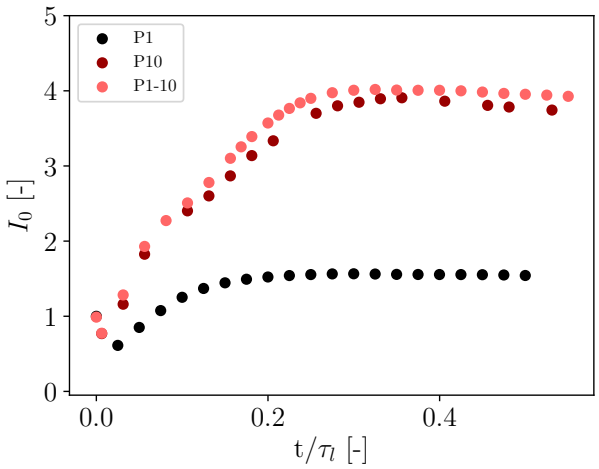

Figure 17: I_0 vs. normalized time for the 3-D cases P1, P10, P1-10 (C5).

laminar flames and are colored by the normalized OH mass fraction. Consistent with earlier observations from the 2-D cases, case P10 displays strong super-adiabaticity of the positively curved flame elements relative to case P1. This is clearly observed from the temperature values shown in Fig. 14 and from OH mass fraction values visualized on the temperature iso-surfaces shown in Fig. 15. Furthermore, case P10 exhibits cellular flame structures to a greater extent than case P1. Consistent with the 2-D DNS results presented above, cases P10 and P1-10 are qualitatively similar, again suggesting that the effects of elevated pressure on lean premixed hydrogen-air flames can be reproduced at atmospheric pressure and controlled by appropriately reducing the unburned reactant temperature and equivalence ratio, i.e., by making the flames *nominally* weaker. The observed qualitative features of the reaction fronts are consistent with predictions from Eq. 1, which are summarized in Tab. 2, showing similar ω_2 values for cases P10 and P1-10, these being larger

than ω_2 for case P1. Figure 16 shows corresponding conditional averages of heat release rate as a function of progress variable and confirms that case P10 displays significantly amplified mean heat release rate compared to P1 with P1-10 behaving in a similar fashion. Figure 17 illustrates the temporal evolution of I_0 that, similarly to the two-dimensional configurations, is more strongly amplified in case P10 compared to case P1, with case P1-10 closely mimicking the former. Therefore, the 3-D DNS cases, while featuring more realistic turbulence-chemistry interaction, clearly confirm the flame behavior observed from the 2-D "pseudo-turbulent" DNS cases, hence illustrating their validity beyond the assumptions and simplifications inherent to the two-dimensional configurations.

Before concluding this section it is important to remark that, although the present turbulence-chemistry interaction results are only based on first-principle numerical simulations, the features of the reaction front (e.g., super-adiabatic finger-like structures) similar to those described above have also been observed in experimental imagery [55] from high-pressure, turbulent premixed hydrogen-air flames.

In conclusion, as a crucial issue for turbulent combustion modeling, the present results suggest that pressure scaling estimates of turbulence-chemistry interaction parameters (Ka, Da), calculated using nominal, one-dimensional flame structure characteristics (strained or unstrained) and *not* taking into account multi-dimensional thermo-diffusive effects, incorrectly characterize turbulent combustion processes for sub-unity Lewis number flames.

5. Discussion on the turbulent burning rate scaling in sub-unity Lewis number flames

As suggested by the analysis of the DNS data that is presented in the previous section, lean premixed H_2-air flames exhibit a dramatic increase in the turbulent burning rate for increasing pressure (cases P1, P10 and P20) everything else being equal, i.e., turbulence-chemistry interaction ($\mathrm{Re_t}$, Da, Ka), reactants temperature (T_u) and composition (ϕ). This scaling is quantified by the significant increase in the stretch factor I_0, shown in Fig. 11 and 17 (for 2-D and 3-D DNS, respectively), that normalizes the turbulent burning rate of lean premixed H_2-air flames with respect to flame surface generation. At this point, before proceeding with this discussion, it is important to note that cases P1, P10 and P20 display an increase in the Zel'dovich number for increasing pressure, i.e., the reactants temperature (and composition) remains unchanged while the crossover temperature (T_0) increases with pressure. Notably, this situation is similar to that encountered by gas turbine manufacturers in more applied R&D efforts aimed to develop and test hydrogen-fired gas turbine combustion systems at high pressure [56] and, crucially, empirical trends observed therein point to a significant augmentation of the burning rate for increasing pressure, ultimately resulting in uncontrolled and potentially harmful flashback events.

However, comparison of the DNS data from all flames spanning across the conditions listed in Tab. 2 and careful inspection of Fig. 18 reveal that the observed I_0 augmentation is not uniquely controlled by pressure itself, but rather by the flame's convection-diffusion-reaction balance. As clearly illustrated by Fig. 18(a), similar I_0 augmentation can be achieved at all pressures

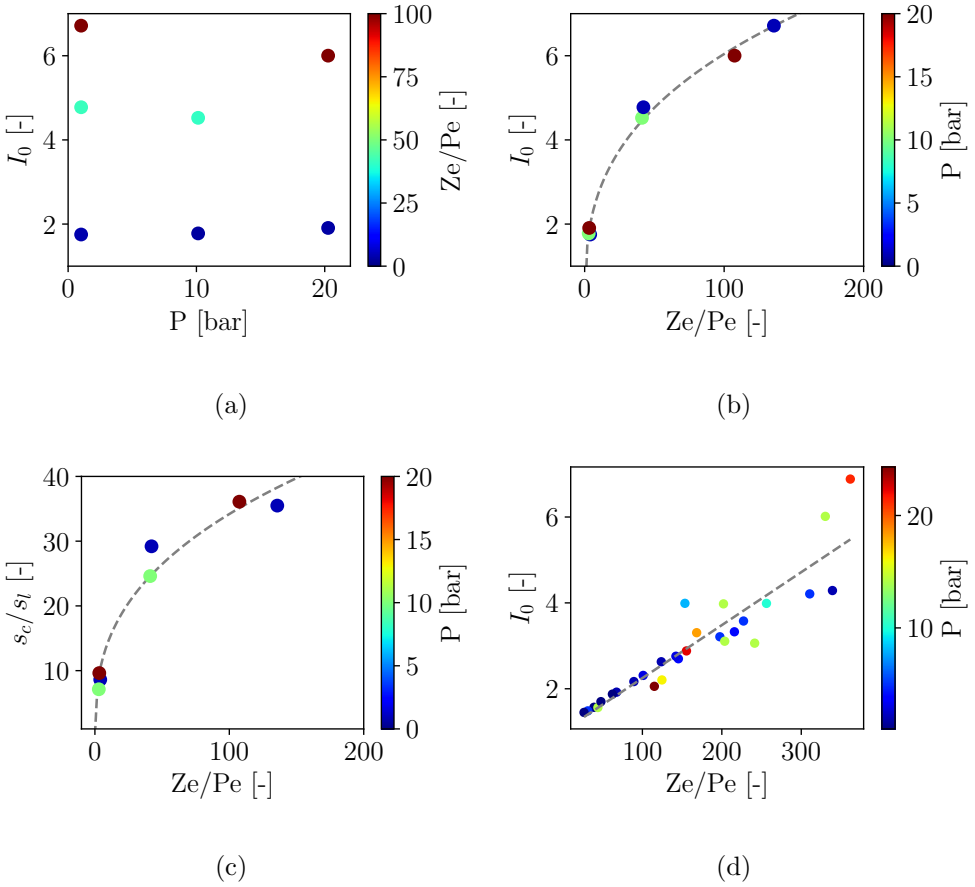

Figure 18: (a): Stretch factor I_0 vs. pressure colored by Ze/Pe (C5), (b): I_0 vs. Ze/Pe colored by pressure (C5), (c) normalized fuel consumption speed s_c/s_l vs. Ze/Pe colored by pressure (C5) and (d) I_0 vs. Ze/Pe colored by pressure (C3).

considered (1, 10 and 20 bar) by opportunely selecting the reactants temperature and composition, i.e., the mixture's thermo-diffusive and thermochemical properties quantified by the parameters Pe, Le, Ma and Ze. While the first three of these parameters represent alternative measures of the relative importance of molecular diffusion in enhancing the flame's tendency to develop thermo-diffusive instabilities, the latter (Ze) is a reflection of the

underlying thermo-chemistry.

In the following, it is assumed that the Peclet number defined according to Eq. 2 most accurately quantifies the importance of molecular diffusion (compared to the conventional Lewis and Markstein numbers) for varying reactants composition, temperature and pressure levels. Then, the following derived parameter, incorporating measures of the flame's reactivity (Ze) and of its tendency to become thermo-diffusively unstable (Pe), is proposed:

$$\wp = \mathrm{Ze}/\mathrm{Pe} \tag{6}$$

and used to scale the stretch factor I_0 extracted from the present DNS data (C5), as shown in Fig. 18(b). The resulting relationship between I_0 and $\wp$ follows a simple power law (dashed line) and accurately incorporates both the turbulent burning rate's direct proportionality to the Zel'dovich number and its inverse proportionality to the Peclet number. A similar trend is also observed for the more "conventional" normalized fuel consumption rate s_c/s_l, as illustrated in Fig. 18(c). In summary, it is concluded that the turbulent burning rate for lean premixed H_2-air combustion, quantified by the stretch factor I_0, becomes large in flames that are characterized by a *larger potential for acceleration* because they are thermo-chemically weaker (larger Ze) and more thermo-diffusively unstable (smaller Pe). Interestingly, the propensity of the parameter $\wp = \mathrm{Ze}/\mathrm{Pe}$ to nearly linearly collapse also the stretch factor I_0 for two-dimensional laminar freely-propagating flames (Configuration C3) is evidenced in Fig. 18(d), indicating its robustness.

Although the major elements of the above discussion are of general validity, it is important to remark that the specific shape of the I_0 scaling represented by the dashed lines in Fig. 18(b) is obtained at constant $\mathrm{Re_t} = 1000$,

Da = 0.1 and Ka = 300 and, consequently, its applicability to different conditions of the turbulence-chemistry interaction needs to be assessed in future work.

6. Conclusions

The effect of pressure on lean premixed hydrogen combustion has been analyzed in various canonical flame configurations including: freely-propagating 2-D laminar premixed flames, 2-D laminar premixed flames subject to monochromatic shear, 2-D premixed flames wrinkled by a synthetic turbulent spectrum and 3-D turbulent flames in homogeneous isotropic turbulence. In all cases investigated, thermo-diffusive instabilities of the flames are clearly amplified with increasing pressure. The amplification is a result of the sensitivity of flame speed and thickness to equivalence ratio variations, with high-pressure flames exhibiting stronger sensitivity to fast molecular diffusion of the hydrogen fuel into the reaction front within the context of a *nominally weaker* combustion process at higher pressure. Two-dimensional direct numerical simulation of premixed laminar flames subjected to shear perturbations demonstrate that, at elevated pressure, flame elements with positive curvature exhibit a clear tendency to become even thinner while the local propagation velocity is more strongly amplified at high pressure compared to atmospheric pressure conditions. Moreover, analysis of two- and three-dimensional direct numerical simulation of turbulent premixed hydrogen-air flames indicates that an increase in pressure leads to a flamelet-like behavior of the entire reaction front with strong super-adiabaticity and acceleration of the positively curved flame elements. Additional DNS calculations fea-

turing selective de-activation of realistic molecular transport, implemented by artificially imposing unity Lewis number, show that molecular diffusion is indeed the key process responsible for acceleration of the flame front at high pressure, confirming previous observations from three-dimensional DNS of highly-turbulent $NH_3/H_2/N_2$-air premixed flames at 1 and 10 bar [33]. Finally, it is shown for the first time that the effects of pressure on the turbulent propagation characteristics of lean premixed hydrogen-air flames can be controlled by opportunely adjusting the reactants temperature and equivalence ratio such that four, rate-controlling dimensionless parameters are matched. In summary, the present study provides the following novel contributions to the field of turbulent premixed combustion of hydrogen-enriched flames:

1. advances the current understanding about the rate-controlling physical mechanisms that ultimately result in a significant acceleration of the flame front, i.e., enhancement of thermo-diffusive instabilities and local enrichment of positively curved portions of the flame front for increasing pressure levels, even in the presence of highly unsteady and intense (broadband) turbulent strain and curvature.
2. proposes a novel Peclet number definition, based on a similar approach compared to that suggested by Howarth & Aspden [43]. This Peclet number is able to capture pressure effects on lean premixed hydrogen-air flames relying on a simple physics-based expression.
3. demonstrates that the quantitative effects of high pressure on the propagation characteristics of lean premixed hydrogen-air flames can be reproduced at atmospheric conditions provided the fresh reactants temperature and equivalence ratio are appropriately adjusted. This result

has significant practical implications, potentially paving the way for experimental observation of high-pressure combustion characteristics at atmospheric conditions where flames are unconfined and diagnostics are more readily applied.

On the basis of the above statements, the present study advances the state-of-the-art, in particular by providing a physics-based explanation of the striking differences observed in the turbulent burning rate of hydrogen-enriched flames for increasing pressure levels.

Ongoing DNS-based research investigates scaling to even higher pressures, and includes parametric studies that examine the impact of varying turbulence intensities and more realistic shear-generated turbulence configurations. Furthermore, future work will focus on modeling efforts that address modifications to the classical premixed flame regime diagram in order to reflect the joint effect of thermo-diffusive instabilities and pressure on sub-unity Lewis number flames and the incorporation of thermo-diffusive effects in turbulence-chemistry interaction models.

Acknowledgments

The work at Sandia National Laboratories was supported by the US Department of Energy, Office of Basic Energy Sciences, Division of Chemical Sciences, Geosciences, and Biosciences. Sandia National Laboratories is a multimission laboratory managed and operated by National Technology and Engineering Solutions of Sandia, LLC., a wholly owned subsidiary of Honeywell International, Inc., for the U.S. Department of Energy's National Nuclear Security Administration under contract DE-NA-0003525. The research

work performed in Norway was supported by the NCCS Centre, performed under the Norwegian research program Centres for Environment-friendly Energy Research of the Research Council of Norway (257579/E20).The authors acknowledge the following partners for their contributions: Aker Solutions, ANSALDO Energia, CoorsTek Membrane Sciences, Gassco, KROHNE, Larvik Shipping, Norcem, Norwegian Oil and Gas, Quad Geometrics, Equinor, TOTAL, and the Research Council of Norway (257579/E20). The computational and data storage allocations on the BETZY supercomputer, granted to the authors by UNINETT Sigma2 - the National Infrastructure for High Performance Computing and Data Storage in Norway (project numbers nn9527k and ns9121k), made this study possible. An award of computer time on Summit at OLCF was provided by the Innovative and Novel Computational Impact on Theory and Experiment (INCITE) program. This research also used resources of the Oak Ridge Leadership Computing Facility, which is a DOE Office of Science User Facility supported under Contract DE-AC05-00OR22725. Research at UCSD has been supported by the AFOSR through Grant # FA9550-16-1-0443.

References

[1] A. Dreizler, H. Pitsch, V. Scherer, C. Schulz, J. Janicka, The role of combustion science and technology in low and zero impact energy transformation processes, App. Energy Combust. Sci. 7 (2021) 100040.

[2] J. Fritz, M. Kröner, T. Sattelmayer, Flashback in a swirl burner with cylindrical premixing zone, ASME J. Eng. Gas Turbine Power 126 (2004) 276–283.

[3] C. Eichler, T. Sattelmayer, Premixed flame flashback in wall boundary layers studied by long-distance micro-piv, Experiments in Fluids 52 (2012) 347–360.

[4] A. Gruber, J. H. Chen, D. Valiev, C. K. Law, Direct numerical simulation of premixed flame boundary layer flashback in turbulent channel flow, J. Fluid Mech. 709 (2012) 516–542.

[5] A. Gruber, E. S. Richardson, A. Konduri, J. H. Chen, Direct numerical simulations of premixed and stratified flame propagation in turbulent channel flow, Phys. Rev. Fluids 3 (2018) 110507.

[6] T. Lieuwen, V. Yang (Eds.), Combustion Instabilities in Gas Turbine Engines, volume 210 of *Progress in Astronautics and Aeronautics*, AIAA, Inc., 2005.

[7] E. Æsøy, J. G. Aguilar, S. Wiseman, M. R. Bothien, N. A. Worth, J. R. Dawson, Scaling and prediction of transfer functions in lean premixed h2/ch4-flames, Combust. Flame 215 (2020) 269 – 282.

[8] R. Magnusson, M. Andersson, Operation of sgt-600 (24 mw) dle gas turbine with over 60 % h2 in natural gas, Proceedings of ASME Turbo Expo 2020: Power for Land, Sea and Air (2020) GT2020–16332.

[9] M. Bothien, A. Ciani, J. Wood, G. Fruechtel, Toward decarbonized power generation with gas turbines by using sequential combustion for burning hydrogen, J. Eng. Gas Turbine Power 141 (2019) 121013–10.

[10] Y. Zeldovich, Theory of combustion and detonation of gases, Acad. Sci. USSR., 1944.

[11] G. Markstein, Cell structure of propane flames burning in tubes, The Journal of Chemical Physics 17 (1949) 428–429.

[12] Y. Zel'dovich, G. Barenblatt, V. Librovich, G. Makhviladze, The Mathematical Theory of Combustion and Explosions, Plenum, New York, 1985.

[13] D. Bradley, C. Sheppart, R. Woolley, D. Greenhalgh, R. Lockett, The development and structure of flame instabilities and cellularity at low markstein numbers in explosions, Combust. Flame 122 (2000) 195–209.

[14] H. Kido, M. Nakahara, K. Nakashima, J. Hashimoto, Influence of local flame displacement velocity on turbulent burning velocity, in: Proceedings 29th International Symposium on Combustion, The Combustion Institute, 2002, pp. 1855–1861.

[15] D. Bradley, M. Lawes, K. Liu, S. Verhelst, R. Woolley, Laminar burning velocities of lean hydrogen–air mixtures at pressures up to 1.0 mpa, Combust. Flame 149 (2007) 162–172.

[16] M. Baum, T. Poinsot, D. Haworth, N. Darabiha, Direct numerical simulation of h2/o2/n2 flames with complex chemistry in two-dimensional turbulent flows, J. Fluid Mech. 281 (1994) 1–32.

[17] J. H. Chen, H. G. Im, Some applications of kolmogorov's turbulence research in the field of combustion, Proc. Comb. Inst. 28 (2000) 211–218.

[18] A. Lipatnikov, J. Chomiak, Molecular transport effects on turbulent

flame propagation and structure, Prog. Energy Combust. Sci. 31 (2005) 1–73.

[19] M. S. Day, J. B. Bell, P.-T. Bremer, V. Pascucci, V. Beckner, M. J. Lijewski, Turbulence effects on cellular burning structures in lean premixed hydrogen flames, Comb. Flame 156 (2009) 1035–1045.

[20] A. J. Aspden, M. S. Day, J. B. Bell, Turbulence-flame interactions in lean premixed hydrogen: transition to the distributed burning regime, J. Fluid Mech. 680 (2011) 287–320.

[21] A. Amato, M. Day, R. Cheng, J. Bell, T. Lieuwen, Leading edge statistics of turbulent, lean, h2–air flames, Proceedings of the Combustion Institute 35 (2015) 1313–1320.

[22] A. Amato, M. Day, R. K. Cheng, J. Bell, D. Dasgupta, T. Lieuwen, Topology and burning rates of turbulent, lean, h2/air flames, Combustion and Flame 162 (2015) 4553–4565.

[23] H. Kobayashi, T. Tamura, K. Maruta, T. Niioka, F. A. Williams, Burning velocity of turbulent premixed flames in a high-pressure environment, Proc. Combust. Inst. 26 (1996) 389–396.

[24] S. Daniele, P. Jansohn, J. Mantzaras, K. Boulouchos, Turbulent flame speed for syngas at gas turbine relevant conditions, Proceedings of the Combustion Institute 33 (2011) 2937–2944.

[25] S. Daniele, J. Mantzaras, P. Jansohn, A. Denisov, K. Boulouchos, Flame front/turbulence interaction for syngas fuels in the thin reaction zone

regime: turbulent and stretched laminar flame speeds at elevated pressures and temperatures, Journal of Fluid Mechanics 724 (2013) 36–68.

[26] S. Wang, A. M. Elbaz, Z. Wang, W. L. Roberts, The effect of oxygen content on the turbulent flame speed of ammonia/oxygen/nitrogen expanding flames under elevated pressures, Combust. Flame 232 (2021) 111521.

[27] P. Venkateswaran, A. Marshall, J. Seitzman, T. Lieuwen, Scaling turbulent flame speeds of negative markstein length fuel blends using leading points concepts, Combust. Flame 162 (2015) 375–387.

[28] L. Berger, A. Attili, H. Pitsch, Intrinsic instabilities in premixed hydrogen flames: Parametric variation of pressure, equivalence ratio, and temperature. part 1-dispersion relations in the linear regime, Combustion and Flame 240 (2022) 111935.

[29] L. Berger, A. Attili, H. Pitsch, Intrinsic instabilities in premixed hydrogen flames: parametric variation of pressure, equivalence ratio, and temperature. part 2–non-linear regime and flame speed enhancement, Combustion and Flame 240 (2022) 111936.

[30] R. Rasool, N. Chakraborty, M. Klein, Effect of non-ambient pressure conditions and lewis number variation on direct numerical simulation of turbulent bunsen flames at low turbulence intensity, Combust. Flame 231 (2021) 111500.

[31] X. Wang, T. Jin, Y. Xie, K. H. Luo, Pressure effects on flame struc-

tures and chemical pathways for lean premixed turbulent h2/air flames: Three-dimensional dns studies, Fuel 215 (2018) 320–329.

[32] Z. Lu, Y. Yang, Modeling pressure effects on the turbulent burning velocity for lean hydrogen/air premixed combustion, Proc. Combust. Inst. 38 (2021) 2901–2908.

[33] M. Rieth, A. Gruber, F. A. Williams, J. H. Chen, Enhanced burning rates in hydrogen-enriched turbulent premixed flames by diffusion of molecular and atomic hydrogen, Combust. Flame (2021) 111740.

[34] M. S. Day, J. B. Bell, Numerical simulation of laminar reacting flows with complex chemistry, Combust. Theory Model. 4 (2000) 535.

[35] J. H. Chen, A. Choudhary, B. de Supinski, M. DeVries, E. R. Hawkes, S. Klasky, W. K. Liao, K. L. Ma, J. Mellor-Crummey, N. Podhorski, R. Sankaran, S. Shende, C. S. Yoo, Terascale direct numerical simulations of turbulent combustion using s3d, Comput. Sci. Discov. 2 (2009) 1–31.

[36] D. G. Goodwin, R. L. Speth, H. K. Moffat, B. W. Weber, Cantera: An object-oriented software toolkit for chemical kinetics, thermodynamics, and transport processes, `https://www.cantera.org`, 2021. doi:`10.5281/zenodo.4527812`, version 2.5.1.

[37] J. Li, Z. Zhao, A. Kazarov, F. L. Dryer, An updated comprehensive kinetic model of hydrogen combustion, Int. J. Chem. Kinet. 36 (2004) 566–575.

[38] G. Jomaas, C. K. Law, J. Bechtold, On transition to cellularity in expanding spherical flames, J. Fluid Mech. 583 (2007) 1–26.

[39] A. Attili, R. Lamioni, L. Berger, K. Kleinheinz, P. E. Lapenna, H. Pitsch, F. Creta, The effect of pressure on the hydrodynamic stability limit of premixed flames, Proc. Combust. Inst. 38 (2021) 1973–1981.

[40] H. Kobayashi, H. Kawazoe, Flame instability effects on the smallest wrinkling scale and burning velocity of high-pressure turbulent premixed flames, Proc. Combust. Inst. 28 (2000) 375–382.

[41] C. Altantzis, C. Frouzakis, A. Tomboulides, M. Matalon, K. Boulouchos, Hydrodynamic and thermodiffusive instability effects on the evolution of laminar planar lean premixed hydrogen flames, J. Fluid Mech. 700 (2012) 329–361.

[42] M. Matalon, C. Cui, J. Bechtold, Hydrodynamic theory of premixed flames: effects of stoichiometry, variable transport coefficients and arbitrary reaction orders, J. Fluid Mech. 487 (2003) 179–210.

[43] T. Howarth, A. Aspden, An empirical characteristic scaling model for freely-propagating lean premixed hydrogen flames, Combust. Flame 237 (2022) 111805.

[44] F. A. Williams, Combustion theory, CRC Press, 1985.

[45] E. R. Hawkes, O. Chatakonda, H. Kolla, A. R. Kerstein, J. H. Chen, A petascale direct numerical simulation study of the modelling of flame wrinkling for large-eddy simulations in intense turbulence, Combust. Flame 159 (2012) 2690–2703.

[46] J. Bechtold, M. Matalon, The dependence of the markstein length on stoichiometry, Combustion and flame 127 (2001) 1906–1913.

[47] R. Addabbo, J. Bechtold, M. Matalon, Wrinkling of spherically expanding flames, Proc. Combust. Inst. 29 (2002) 1527–1535.

[48] K. N. C. Bray, R. S. Cant, Some applications of kolmogorov's turbulence research in the field of combustion, Proc. Roy. Soc. Lond. 434 (1991) 217–240.

[49] E. Hawkes, J. H. Chen, Direct numerical simulation of hydrogen-enriched lean premixed methane–air flames, Comb. Flame 138 (2004) 242–258.

[50] A. Lipatnikov, J. Chomiak, Turbulent flame speed and thickness: phenomenology, evaluation, and application in multi-dimensional simulations, Prog. Energy Comb. 28 (2002) 1–74.

[51] S. Chaudhuri, V. Akkerman, C. K. Law, Spectral formulation of turbulent flame speed with consideration of hydrodynamic instability, Physical Review E 84 (2011) 026322.

[52] R. Feng, A. Gruber, J. H. Chen, D. M. Valiev, Influence of gas expansion on the propagation of a premixed flame in a spatially periodic shear flow, Combust. Flame 227 (2021) 421–427.

[53] H. G. Im, J. H. Chen, Effects of flow transients on the burning velocity of laminar hydrogen/air premixed flames, Proceedings of the Combustion Institute 28 (2000) 1833–1840.

[54] N. Peters, Turbulent Combustion, Cambridge University Press, 2000.

[55] S. Yang, A. Saha, W. Liang, F. Wu, C. K. Law, Extreme role of preferential diffusion in turbulent flame propagation, Combust. Flame 188 (2018) 498–504.

[56] B. Emerson, D. Wu, T. Lieuwen, S. Sheppard, D. Noble, L. Angello, Assessment of current capabilities and near-term availability of hydrogen-fired gas turbines considering a low-carbon future, in: Proceedings of ASME Turbo Expo 2020: Power for Land, Sea and Air, September 21-25, 2020, Virtual, Online, 2020, pp. GT2020–15714.